

Gamma ray attenuation in X-Ray binaries: An application to $LSI + 61^\circ 303$

Paul D. Nuñez, Stephan LeBohec, Stephane Vincent

*Dept. of Physics & Astronomy
University of Utah
115 S 1400 E, Salt Lake City, UT, USA.*

ABSTRACT

The X-ray binary $LSI + 61^\circ 303$, consisting of a main sequence Be star and a compact object has been detected in the TeV range with MAGIC and VERITAS, and showed a clear intensity modulation as a function of the orbital phase. We describe a gamma-ray attenuation model and apply it to this system. Our first result is that interaction of high energy photons with the background radiation produced by the main sequence star alone does not account for the observed modulation. We then include interactions between very high energy radiation and matter, and are able to constrain fundamental parameters of the system such as the mass of the compact object and the density of circumstellar matter around the Be star. In our analysis of the TeV data, we find that the compact object has mass $M_2 > 2.5M_\odot$ at the 99% confidence level, implying it is most likely a black hole. However, we find a column density which conflicts with results from X-ray observations, suggesting that attenuation may not play an important role in the modulation.

1. Introduction

In the past few years, several high mass X-ray binaries have been detected as gamma ray emitters (Aharonian et al. 2006; Albert J., et al. 2006; Acciari et al. 2008), causing an intensification of observational and theoretical interest. High energy emitting binary systems consisting of a main sequence star and a compact object are the only known very high energy (VHE) galactic variable sources, and their short periods of days or weeks make them even more interesting observational targets. With increasing spectral coverage and statistics, the nature of photon emission and absorption mechanisms is becoming increasingly constrained. Here we are concerned with high energy (TeV) photons emitted from the vicinity of the compact object and interacting with the background black body radiation and ejected material from the companion star. Even though these systems can be incredibly complex, a simple model of the absorption mechanisms and how they affect the system's light curve, can still shed light on many aspects such as the compact object mass and the orbital parameters.

One such example is the high energy emitting binary *LS I + 61°303* (Massi, et al. 2004). It was first detected in the TeV range with MAGIC (Albert J., et al. 2006) and further observed with VERITAS at flux levels ranging between 5% and 20% of the Crab Nebula (Acciari et al. 2008). This source has been observed throughout most of the electromagnetic spectrum starting with radio frequencies and extending to VHE gamma rays (Leahy 2004). This broad spectral study indicates that the system consists of a main sequence Be star of mass $M_1 = 12.5 \pm 2.5 M_\odot$ (Casares, et al. 2005), surrounded by a circumstellar disk (Grundstrom et al. 2007; Paredes et al. 2007), and a compact companion separated by tens of solar radii at periastron. The compact companion can be either a neutron star or a black hole (Casares, et al. 2005), and its exact nature is still subject of investigation and debate (Zdziarski et al. 2010). The maximum VHE emission occurs close to apastron (Acciari et al. 2008; Albert J., et al. 2006), suggesting that absorption plays an important role in the modulation.

The outline of the paper is as follows: first we describe the model of attenuation due to pair production. Then we consider the particular case of LS I +61 303. We assume that the high energy radiation is emitted from the vicinity of the compact object and that its emission is isotropic and constant in time. The modulation due to photon-photon interactions is found to be insufficient to account for the VERITAS observations. For this reason, we include additional interactions of VHE photons with circumstellar material. This model permits to constrain the orbital parameters and the mass of the compact object as well as the density of ejected material from the companion star.

2. Interaction with background radiation

2.1. Radiative transfer equation

The radiative transfer equation (Chandrasekhar 1960) for the intensity $I(s, E)$, where s is the distance traveled by a photon of energy E from the emission point is

$$\frac{dI(s, E)}{ds} = -(1 - \cos \xi) n(s, \epsilon) \sigma(E, \epsilon, \xi) I(s, E) + j(s, E) ; \quad (1)$$

Where $n(s, \epsilon)$ is the spectral density of background photons of energy ϵ emitted by the main sequence star, $\sigma(E, \epsilon, \xi)$ is the cross section¹ for the interaction between photons colliding at angle ξ , and $j(E, s)$ is a source term.

¹Note that the term $(1 - \cos \xi(s'))$ corresponds to the relative velocity between the incident and target photons

2.2. Neglecting the source term

The source term corresponds to secondary gamma-rays in the electromagnetic cascade. We can estimate the effect of the source term in the context of a cascade toy model, where the energy of these secondary gamma-rays is degraded by typically a factor of 4 (after the primary photon first produces an e^+e^- pair). Consequently, the increase in the intensity $I(s, E)$ of gamma rays of energy E is increased by $2\tau I(s, 4E) + \mathcal{O}(\tau^2)$, where τ is the probability of interaction (or optical depth as defined in section 2.3). Assuming a power spectrum (section 4) we note that $I(s, 4E) = I(s, E)4^{-\gamma}$. The source term is then approximately given by

$$j(s, E) \approx 2 \times 4^{-\gamma} n(s, \epsilon) \sigma(E, \epsilon, \xi) I(s, E). \quad (2)$$

In this order of magnitude approximation, we have assumed that the cross section is the same for the energies E and $4E$. In the TeV range, the cross section decreases as $\sim (\epsilon E)^{-1} \ln \epsilon E$ (Aharonian 2004), therefore eq. 2 constitutes an upper bound. Now taking $\gamma \sim 2$, we note that the source term is smaller than the attenuation term in eq. 1 by a factor of $\lesssim 10$. Consequently, we neglect the source term (For a detailed numerical calculation, see, e.g. Sierpowska & Bednarek (2005)).

2.3. Solution of the Radiative transfer equation

With the source term neglected, the solution to the radiative transfer equation is

$$I(s, E) = I(s_0, E) \exp \left\{ - \int_{s_0, \epsilon}^{\infty, \infty} (1 - \cos \xi(s')) n(s', \epsilon') \sigma(E, \epsilon', s') ds' d\epsilon' \right\}. \quad (3)$$

Here s_0 is the emission point in the vicinity of the compact object (see figure 1), and ϵ corresponds to the threshold energy for pair production,

$$\epsilon = \frac{2m_e^2 c^4}{E(1 - \cos \xi(s))}. \quad (4)$$

The dependence of the scattering angle ξ in eq. 3 has been changed to a dependence on the path s . The problem then reduces to calculating the integral in the exponential of eq. 3, also known as the optical depth $\tau(s, E)$ (Ribicki & Lightman 1979). In our calculation, we consider the main sequence star as a point source, and in view of the results obtained by Dubus (2006), including the angular extension does not change our results significantly.

The distribution of background black body photons can be taken as

$$n(r, \epsilon) = n_0(\epsilon) \frac{r_0^2}{r^2}, \quad (5)$$

where r_0 and n_0 are the radius of the Be star and the density of background photons at this radius, i.e.

$$n(r, \epsilon) = \frac{2\pi \epsilon^2 d\epsilon}{c^3 h^3} \left(\frac{r_0}{r}\right)^2 \frac{1}{e^{\epsilon/kT} - 1}. \quad (6)$$

Here, the photon density has already been integrated over the solid angle.

3. The case of LS I+61 303

3.1. Attenuation

There is debate as to what is the mechanism responsible for high energy emission. However, the aim of this paper is not to model the gamma ray emission but rather to investigate the effects of attenuation. This allows to derive a few characteristics of the main sequence star environment and compact object orbit.

Grundstrom et al. (2007) reported a temperature of $T \approx 3 \times 10^4 K$ and radius of $R \approx 6.7R_\odot$ for the Be star. The black body distribution peaks at a few eV, and the threshold energy for pair production with TeV incident photons is of the order of 1 eV, so that most of the background photons may contribute to the attenuation, provided the scattering angle is favorable. The background photon density is found to be of the order of $n_\gamma \sim 10^{12} \text{ cm}^{-3}$ at the radius of the star. The circumstellar disk has been observed by Waters et al. (Waters et al. 1988) and by Paredes et al. (Paredes et al. 2007), who estimate the disc ion density to be $n_e \sim 10^{13} \text{ cm}^{-3}$ at one stellar radius. The cross section for pair production is of the order of $\sigma_{\gamma\gamma} \approx 0.1\sigma_T$ at the threshold energy. The cross section for interaction with hydrogen has a constant value of $\sigma_{\gamma H} \approx 2 \times 10^{-2}\sigma_T$ above a few hundred MeV (Heitler 1954; Aharonian 2004). With these cross sections, a first estimate suggests that both interactions may result in comparable degrees of attenuation. However, there is a strong angular dependence in the $\gamma\gamma$ interaction, the extreme case being when the both photons are emitted in the same direction, a configuration in which there is no VHE attenuation. Also the threshold energy is much higher when the incident and target photons are nearly parallel, so fewer background photons contribute to attenuation. Consequently, $\gamma\gamma$ attenuation may not have strong modulation as a function of the orbital phase when compared with the modulation produced by interactions with the circumstellar material.

3.2. Orbital parameters of $LSI + 61^\circ 303$

The orbital parameters of $LSI + 61^\circ 303$, as sketched in figure 1, are still subject of research (Aragona et al. 2009; Grundstrom et al. 2007; Casares, et al. 2005). The quantities of interest are: the period P , the angle between the major axis of the ellipse and the line of sight ψ , the projected semi-major axis ($a_1 \sin i$), corresponding to the ellipse of the Be star², the eccentricity η , the phase at periastron ϕ_0 , and the mass function $f(M_1, M_2)$, which depends on the period and the radial velocity and relates the masses of both objects and the inclination angle i . The most recent orbital solution has been obtained by Aragona et al. (2009), where $P = 26.4960 d$, $\psi = 40.5 \pm 5.7^\circ$, $a_1 \sin i = 8.64 \pm 0.52 R_\odot$, $\eta = 0.54 \pm 0.03$, $\phi_0 = 0.275$ and $f(M_1, M_2) = 0.0124 \pm 0.0022 M_\odot$. Assuming the attenuation is responsible for the periodic modulation of the TeV emission, our results constrain i and thereby the mass of the compact object.

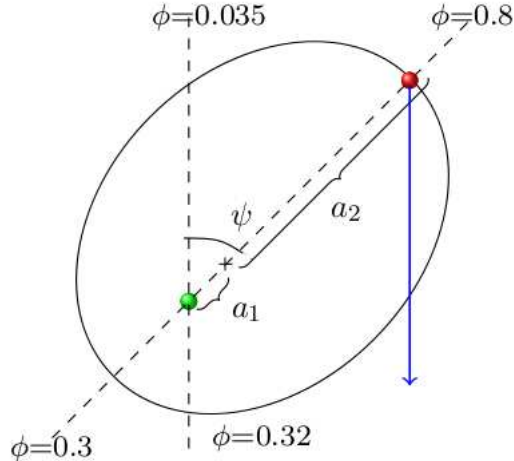


Fig. 1.— Sketch of the orbital parameters of $LSI + 61^\circ 303$ for the case of $i = 90^\circ$. The arrow points to the observer. Also shown are the values of the phase at periastron, apastron, and superior and inferior conjunction.

4. The integrated flux

Following observations of $LSI + 61^\circ 303$ from 09/2006 to 02/2008, the VERITAS collaboration reported power law spectrum ($\frac{d\Phi}{dE} = \Phi_0 \left(\frac{E}{TeV}\right)^{-\gamma}$) with a spectral index of $\gamma = 2.4 \pm 0.2_{stat} \pm 0.2_{syst}$ at energies above ~ 0.5 TeV, and between phases $\phi = 0.6$ and $\phi = 0.8$ (Acciari et al. 2008). Observations at lower energies made by Fermi between 08/2008 and 03/2009, indicate that the

²The projected semi-major axis of the ellipse described by the compact object is typically labeled as $a_2 \sin i$.

spectral index does not change significantly as a function of the orbital phase (Abdo et al. 2009). Therefore, we assume a constant intrinsic³ spectrum as a function of the phase at TeV energies. The integrated flux is then

$$F(\phi) = \int_{E_0}^{\infty} \frac{d^3N}{dEdtdA} I(E, \phi) dE = F_0 \int_{E_0}^{\infty} \left(\frac{E}{E_0} \right)^{-\gamma} I(E, \phi) dE, \quad (7)$$

where E_0 depends on the detection threshold energy of the detector, and F_0 is a normalization factor that is taken as a free parameter.

4.1. Light curve assuming only $\gamma\gamma$ interactions

Figure 2 shows the attenuation as a function of the orbital phase for several different energies for the case of the compact object having the canonical neutron star mass ($i \approx 64^\circ$ or $M \approx 1.5M_\odot$). In figure 2 we essentially reproduce one of the results obtained by Dubus, except that the orbital parameters used are the newer set obtained by Aragona et al. (2009). When only interactions with the background black body photons are taken into account, and the orbital plane is closer to being seen edge-on, the optical depth approaches a minimum when the compact object is close to the main sequence star. This is especially the case for very high inclination angles, corresponding to the mass of the compact object being small, and close to the Chandrasekhar mass. This behavior can be understood from the angular dependence of the threshold energy in addition to the relative velocity of the incident and target photons approaching a minimum. Also, at high energies, the cross section for pair creation decreases as the inverse square of the center of mass energy, decreasing the optical depth even more. That is, even though the total density of background photons increases (as $1/r^2$) when the compact object approaches the Be star, a combination of the previously mentioned factors dominates as can be seen in figure 2.

Figure 3 shows the normalized integrated flux assuming different inclination angles and corresponding compact object masses. The VERITAS data shown in figure 3 (Weinstein et al. 2008) were binned to show a single light-curve as opposed to monthly data. If we assume that the emission comes from the vicinity of the compact object, and is isotropic, and constant as a function of the orbital phase, then these results lead us to conclude that there must be an additional attenuation mechanism at play.

³By intrinsic we mean non attenuated by pair production.

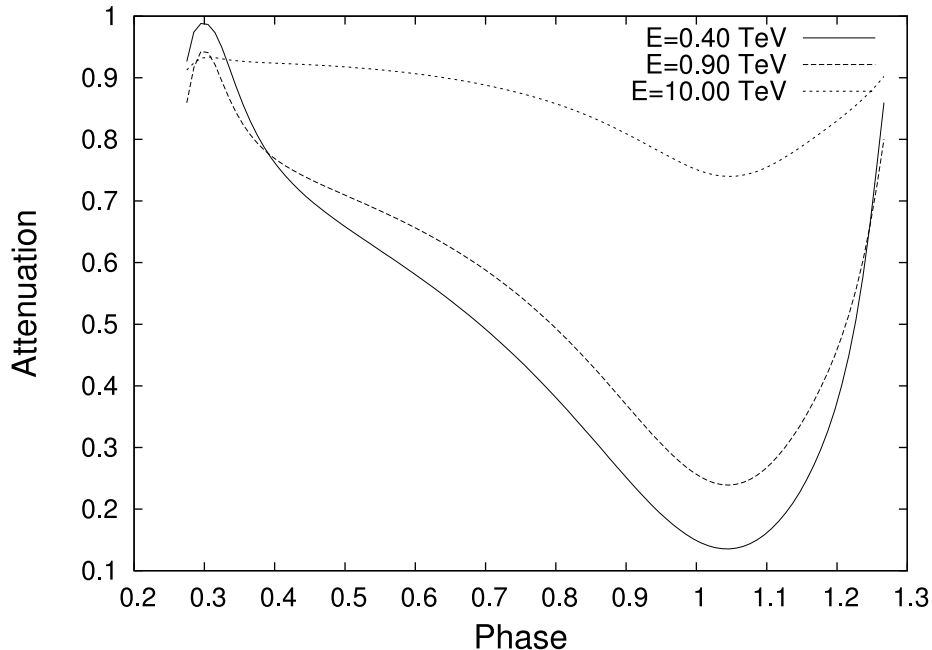


Fig. 2.— Attenuation $e^{-\tau_{\gamma\gamma}}$ as a function of the orbital phase for different primary photon energies ($\gamma\gamma$ interactions only). A mass of $1.5M_{\odot}$, corresponding to $i = 64^{\circ}$, was assumed for the compact object.

4.2. Light curve including $\gamma\gamma$ and γH interactions

The detailed structure of the circumstellar material surrounding a Be star in the presence of a compact companion has been studied by Waters et al. (1988), Marti & Paredes (1995) and Reig et al. (2000) among others. It is thought to consist of a main equatorial disk-like component and a polar wind. Typically, the parameters that describe the decretion disk include: the mass loss rate, the wind termination velocity, the half opening angle of the disk, and radius of the disk. The polar wind is radiatively driven and may have a corresponding mass loss rate comparable to the equatorial wind (within one order of magnitude (Waters et al. 1988)). When comparing the quality of the data shown in figure 3, and the complexity of the models that describe the circumstellar material, it appears that, when only TeV data is used, only an order of magnitude estimate of the material density and its extension in the system can be achieved. With this in mind, we rather assume a simple isotropic distribution of material that decreases as a power q of the distance from the Be star ($n = n_H(r_0/r)^q$). We start by setting $q = 2$ and then consider different values for comparison. Parameters found from existing models are taken into consideration for our approximation.

For the case of a constant cross section and a $1/r^2$ distribution of hydrogen, the optical depth can actually be found analytically (see appendix A). The resulting light curves are shown in figure

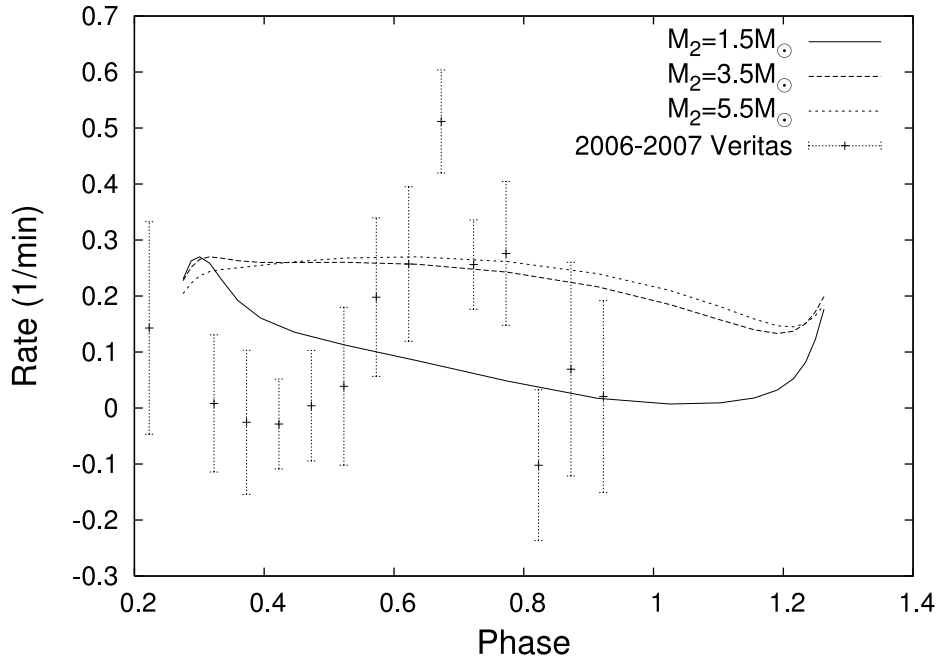


Fig. 3.— Normalized light-curve for $\gamma\gamma$ interactions only. Each curve corresponds to a different mass of the compact object and inclination angle.

4 for different values of the inclination angle. For low inclination angles (high mass), VHE photons emitted from apastron go through less circumstellar hydrogen than those emitted from periastron. This results in minimum attenuation near apastron, as can be seen in figure 4. From this figure it is clear that the emission peak corresponding to a canonical $1.5M_{\odot}$ neutron star is only marginally supported by observations.

We take the inclination angle, characteristic density, and normalization factor as free parameters. We find the inclination angle to be $i < 28^{\circ}$ ($M_2 > 3M_{\odot}$) at the 89% confidence level (CL) in the context of this model, and $i < 34^{\circ}$ ($M_2 > 2.5M_{\odot}$) at the 99% CL. These limits are not in good agreement with the neutron star scenario generally favored for the broad-band spectrum it implies⁴. However, our results are still consistent with other observational constraints ($10^{\circ} < i < 60^{\circ}$) (Casares, et al. 2005) obtained from optical spectroscopy. As for the circumstellar material, if we assume the characteristic extension to be $r_0 \approx 100R_{\odot}$, consistent with more sophisticated models (Sierpowska-Bartosik & Torres 2009), then the density of hydrogen in the disk is found to be $2.0 \times 10^{13} \text{cm}^{-3} \leq n_H \leq 1.9 \times 10^{15} \text{cm}^{-3}$ at the 99% CL and $n_H = (2.7 \pm_{2.1}^{11.3}) \times 10^{14} \text{cm}^{-3}$ at the 68%

⁴See Zdziarski et al. (Zdziarski et al. 2010) for more details

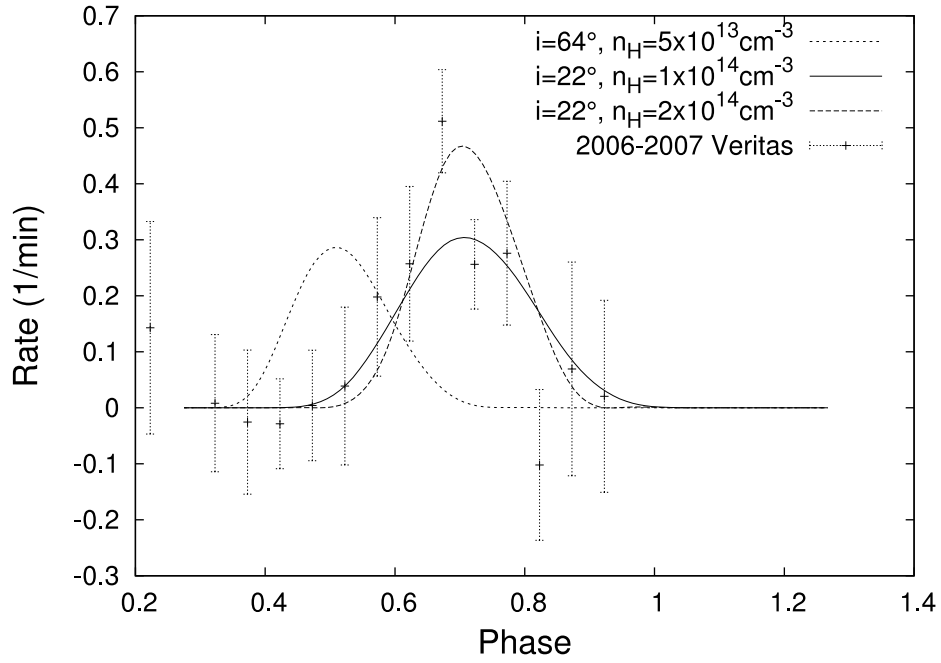


Fig. 4.— Light curves for different inclination angles i and hydrogen densities n_H when an isotropic distribution of hydrogen is included. The mass of the compact object is $4.0M_\odot$ for the two curves whose peak is at phase ~ 0.7 , and $1.5M_\odot$ for the curve whose peak is closer to phase ~ 0.4 . The concentration of hydrogen at $r \approx 100R_\odot$ for each curve is labeled in the top right-hand corner of the figure. In the two right-most curves, the intrinsic luminosity (normalization factor) is chosen so as to maximize agreement with data, and it increases with the hydrogen density.

CL.

By integrating the volume density along the line of sight to the compact object at apastron, we find a column density of $1.9 \times 10^{26} \text{cm}^{-2} \leq N_{\text{H}} \leq 1.8 \times 10^{28} \text{cm}^{-2}$ at the 99% CL, which is much higher than results found elsewhere in the literature (Waters et al. 1988; Marti & Paredes 1995; Esposito et al. 2007). In particular, when we use the column density found by X-ray observations $N_{\text{H}} = (5.7 \pm 0.3) \times 10^{21} \text{cm}^{-2}$ Esposito et al. (2007), we find a reduced $\tilde{\chi}^2$ of 3.06 (11 degrees of freedom), corresponding to a χ^2 probability $P(\tilde{\chi}^2 \geq 3.06) = 0.04\%$. A rough estimate suggests that by including $\sim 10\%$ of helium, the column density would be reduced by a factor of ~ 2 , which is not sufficient to achieve compatibility with X-ray results.

Density profiles in Be stars typically have radial dependences of $1/r^q$, where $2.3 < q < 3.3$ (Lamers & Waters 1987), depending on the opening angle of the disk. Therefore we expect our constraint on the density to constitute a lower bound⁵. We perform our calculation with $q = 3$ and note that our results do not change considerably.

The hydrogen density also corresponds to a mass loss rate of $\dot{M}_1 \approx 10^{-7} \Omega \frac{V_{\text{wind}}}{1 \text{km s}^{-1}} M_{\odot} \text{yr}^{-1}$, where Ω is the solid angle. Typically accepted values for the mass loss rate are in the range of $\sim 10^{-7} M_{\odot} \text{yr}^{-1}$ to $10^{-8} M_{\odot} \text{yr}^{-1}$, as have been reported by Snow (1981) and Waters et al. (1988) among others. A first glance at our result for the mass loss implies that it does not agree with the observations, i.e. setting $\Omega = 4\pi$ and $V_{\text{wind}} \sim 100 \text{km s}^{-1}$ (Waters et al. 1988). However, if we relax the assumption of an isotropic distribution of hydrogen, our result implies that small solid angles are favored as well as small velocities for the stellar wind. Small solid angles are consistent with the thin disk scenario that is most commonly accepted. Small velocities of the order of a few km s^{-1} are however not consistent with what is found elsewhere in the literature, e.g. (Waters et al. 1988), and the wind indeed has higher velocities, this would imply that the system may have been observed while in a state of high mass loss rate.

5. Discussion

Since, in the TeV range, the interaction with matter is approximately independent of the energy, and since, as figure 3 shows, $\gamma\gamma$ interactions are insufficient to account for the orbital modulation, then the intrinsic non-attenuated differential spectrum is essentially the same as the observed spectrum (a power law of spectral index -2.4). However, the intrinsic TeV luminosity is several orders of magnitude higher than the measured luminosity. Taking the distance to

⁵This is assuming that the disk and orbit lie in the same plane.

the source to be approximately 1.8 kpc (Steele et al. 1998), we find the intrinsic luminosity to be $L \approx 5 \times 10^{37} \text{ergs}^{-1}$ when the hydrogen density is of the order of $\sim 5 \times 10^{13} \text{cm}^{-3}$. This intrinsic luminosity is comparable to that suggested by Bottcher (2007) for *LS 5039*, the only other known TeV binary thought to contain a black hole.

It is interesting to compare this intrinsic luminosity to the Eddington luminosity⁶ $L_{Edd} \approx 1.3 \times 10^{39} (M_2/M_\odot) \text{ergs}^{-1}$, which is comparable to L , and implies that radiation may be beamed in our direction. It is also interesting to calculate the accretion rate that would be needed in order to obtain the intrinsic luminosity: By taking $L \approx GM_2\dot{M}_2/R$, where R is of the order of the Schwarzschild radius ($2GM_2/c^2$), we find $\dot{M}_2 \approx 2 \times 10^{-8} M_\odot \text{yr}^{-1}$. This rate is comparable with the observed mass loss rate of $\sim 10^{-8} M_\odot \text{yr}^{-1}$. The fact that the accretion rate is comparable to the measured mass loss rate, suggests that the flow of matter can be quite complicated, e.g. an increase in the accretion rate would strip most of the circumstellar mass, leading to time variability. This may explain the fact that no VHE detections have been reported since 2008.

Still assuming the intrinsic luminosity to be constant in time, we can estimate the amount of hydrogen needed to attenuate the source to below the detectability threshold. We find that the density must increase from $\sim 5 \times 10^{13} \text{cm}^{-3}$ to $\sim 5 \times 10^{14} \text{cm}^{-3}$ at the characteristic distance of $100R_\odot$. This amount of hydrogen in turn leads to much higher mass loss rates than those observed, and it may also imply a stronger activity of the source.

It is worth mentioning that the attenuation model is not the only possible way to account for the modulation. For example, there is also the possibility of the emission being anisotropic, and the modulation resulting from a geometrical effect. This possibility is described in detail by Zdziarski et al. (2010), where a shocked pulsar wind with a large Lorentz factor is thought to be the cause of emission.

6. Conclusions

For the case of *LS I + 61°303*, we find that attenuation due to $\gamma\gamma$ interactions with the background radiation does not account for the observed high energy flux modulation as a function of the orbital phase, namely a narrow peak near apastron. This effect leads us to investigate some properties of the ejected material from the Be star, and the inclination angle of the orbit. We find the angle of the orbit to be $i < 34^\circ$ ($M > 2.5M_\odot$) at the 99% confidence level, suggesting that the compact object is a black hole rather than a neutron star. We also find the density of hydrogen in the disk to be $2 \times 10^{13} \text{cm}^{-3} \leq n_{\text{H}} \leq 2 \times 10^{15} \text{cm}^{-3}$ at the 99% CL (at $100R_\odot$), which

⁶At the energies considered here, the cross section for inverse Compton is $\sim 0.1\sigma_T$

accounts for most of the observed gamma ray absorption. If the compact object is indeed a black hole as our analysis suggests, then the gamma ray emission is likely to be powered by accretion (Bosch-Ramon et al. 2006; Zdziarski et al. 2010). Also, a black hole scenario might be even more complicated due to the possibility of VHE emission originating from termination of jets, therefore we cannot exclude the possibility of the modulation being due to geometrical effects. Current VHE data does not allow to constrain the system much more than what we have already done, and the fact that VHE detections have not been reported since the VERITAS (Acciari et al. 2008) and MAGIC (Albert J., et al. 2006) detections where made, makes the problem even more puzzling. A possible explanation might originate from a complex matter flow. This is suggested by the fact that the accretion rate needed to explain an intrinsic non-attenuated luminosity, is comparable to the measured mass loss rate of the Be star.

An inconsistency arises when comparing our results with those derived from X-ray observations. We find the column density to be $1.9 \times 10^{26} \text{cm}^{-2} \leq N_{\text{H}} \leq 1.8 \times 10^{28} \text{cm}^{-2}$ (99% CL), which is only compatible with X-ray results at the 0.04% confidence level. Such an incompatibility may imply that pair production in the stellar wind is not the cause of the modulation. Consequently, our estimates on the mass and column density may not be valid. An alternative explanation by Zdziarski et al. (2010) suggests that the modulation is due to a geometrical effect. Here a shocked pulsar wind is thought to flow along a cone with a large Lorentz factor, producing beamed radiation which can be seen when the cone passes through the line of sight.

Appendix A: Optical depth for constant cross section and $1/r^2$ density distribution

Using a $1/r^2$ distribution of hydrogen, the cross section σ_H accounting for interactions between VHE photons and hydrogen, and the system of coordinates shown in figure 5 (corresponding to an orbital plane seen edge on) , we can calculate the integral for the optical depth to be

$$\int_{x_i}^{\infty} \frac{n_H r_0^2 \sigma_H}{x^2 + y_i^2 + z_i^2} dx = \left[\frac{n_H r_0^2 \sigma_H}{\sqrt{y_i^2 + z_i^2}} \tan^{-1} \left(\frac{x}{\sqrt{y_i^2 + z_i^2}} \right) \right]_{x_i}^{\infty} \quad (8)$$

$$= \frac{n_H r_0^2 \sigma_H}{\sqrt{y_i^2 + z_i^2}} \left(\frac{\pi}{2} - \tan^{-1} \left(\frac{x_i}{\sqrt{y_i^2 + z_i^2}} \right) \right), \quad (9)$$

where x_i , y_i , and z_i are functions of the orbital angle θ , and r_0 is the characteristic radius of the hydrogen disk. For the case of a circular orbit as seen edge on (figure 5), we can easily see the limiting behavior of the intensity as a function of the orbital angle. That is, expanding around $\theta \sim 0$ reveals that the attenuation around this region behaves like a Gaussian.

$$\text{For } \theta \sim 0 : I(r_i, \theta) = I_0(\theta, r_i) e^{-\frac{n_H r_0^2 \sigma_H}{r_i} (1+\theta^2)}. \quad (10)$$

Similarly, expanding around $\theta \sim \pi/2$ reveals that the attenuation behaves like a decreasing exponential

$$\text{For } \theta \sim \pi/2 : I(r_i, \theta) = I_0(\theta, r_i) e^{-\frac{n_H r_0^2 \sigma_H}{r_i} \theta} \quad (11)$$

For a more complicated geometry of *LSI + 61°303*, it is now just a matter of inserting the appropriate expressions for $x_i(\theta)$, $y_i(\theta)$ and $z_i(\theta)$.

REFERENCES

- Abdo, A. A., et al. 2009, *ApJ*, 701, L123
- Acciari V. A. et al. 2008, *Apj*, 665, L51
- Aharonian, F. 2004, Singapore: World Scientific Publishing Co.
- Aharonian, F., et al. 2006, *A&A*, 460, 743
- Albert J., et al. 2006, *Science* 312, 1771
- Aragona, C., McSwain, M. V., Grundstrom, E. D., Marsh, A. N., Roettenbacher, R. M., Hessler, K. M., Boyajian, T. S., & Ray, P. S. 2009, *ApJ*, 698, 514
- Bottcher, M. 2007, *Astroparticle Phys*, 27, 278
- Bosch-Ramon et al. 2006, *A&A*, 459, L25
- Casares J., Ribas I., Paredes J. M., Martí J., Allende Prieto C. 2005, *MNRAS*, 360, 1105
- Chandrasekhar, S. 1960, New York: Dover, 1960
- Dubus G. 2006, *A&A*, 451, 9.
- Esposito, P., et al. 2007, *A&A*, 474, 575
- Gould R. J. & Schröder G. P. 1967, *Phys. Rev.*, 155, 1404
- Grundstrom E. D. et al. 2007, *ApJ* 656 437
- Heitler, W. 1954, Oxford: Clarendon Press.
- Jauch, J. M. & Rohrlich, F. 1980, New York: Springer-Verlag.

- Lamers H. J. G. L. M., Waters L. B. F. M. 1987, *A&A*, 182 80
- Leahy D. A. 2004, *A&A* 413, 1019-1028
- Martí J. & Paredes J. M. 1995, *A&A*, 298, 151
- Massi M., Paredes, J. M., Garrington, S. T., Peracauta, M., & Marti, J., 2004, *A&A*, 414, L1
- Paredes, J. M., Ribó, M., Bosch-Ramon, V., West, J. R., Butt, Y. M., Torres, D. F., & Martí, J. 2007, *ApJ*, 664, L39
- Reig et al. 2000, *MNRAS*, 317, 205
- Sierpowska-Bartosik, A., & Torres, D. F. 2009, *ApJ*, 693, 1462
- Sierpowska, A., & Bednarek, W. 2005, *MNRAS*, 356, 711
- Snow T. P. 1981, *ApJ*, 251, 139
- Steele, I. A., Negueruela, I., Coe, M. J., & Roche, P. 1998, *MNRAS*, 297, L5
- Ribicki G. B. & Lightman A. P. 1979, New York: Wiley, 1979
- Waters et al. 1988, *A&A*, 198, 200
- Weinstein et al. 2008, *Acta Phys. Polon. Supp*, 1, 595
- Zdziarski A. A.; Neronov, A., Chernyakova M. 2010, *MNRAS*, 403, 4, 1873

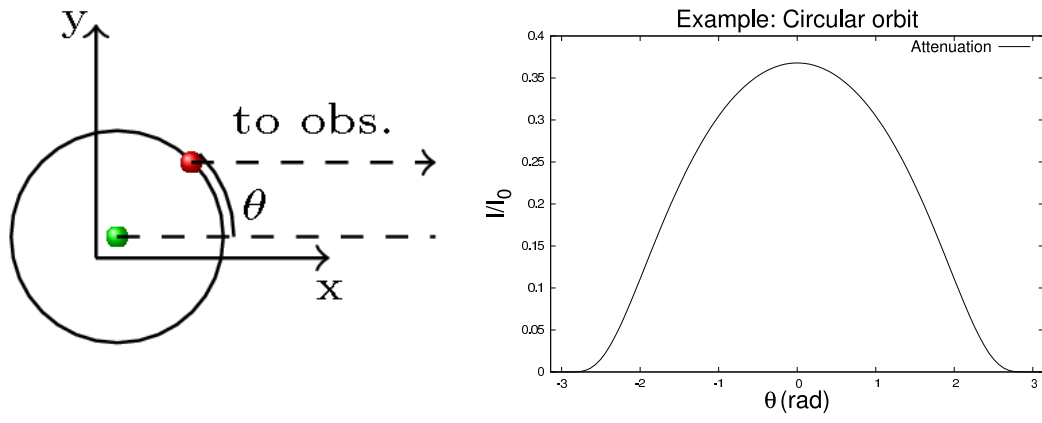


Fig. 5.— Coordinate system used for calculating the optical depth (eq. 9).